Optogenetic Multiphysical Fields Coupling Model for Implantable Neuroprosthetic Probes.

IEEE Access
Multidisciplinary | Rapid Review | Open Access Journal

Received 15 July 2024, accepted 5 August 2024, date of publication 12 August 2024, date of current version 20 September 2024.

Digital Object Identifier 10.1109/ACCESS.2024.3441571

RESEARCH ARTICLE

Optogenetic Multiphysical Fields Coupling Model for Implantable Neuroprosthetic Probes

NA DONG[1], EMILY JOHNSON[2], ROLANDO BERLINGUER-PALMINI[2], HONGZE ZHONG[3], FAHIMEH DEHKHODA[3], AHMED SOLTAN[4], KONSTANTIN NIKOLIC[5], (Member, IEEE), NIR GROSSMAN[6], JOHANNES GAUSDEN[3], RICHARD BAILEY[3], ANTHONY O'NEILL[3], (Senior Member, IEEE), ANDREW JACKSON[2], ANDREW TREVELYAN[2], PATRICK DEGENAAR[3], (Senior Member, IEEE), AND XIAOHAN SUN[1]

[1]National Research Centre for Optical Sensing/Communication Integrated Networking, Southeast University, Nanjing 210096, China
[2]Faculty of Medical Sciences, Newcastle University, NE1 7RU Newcastle upon Tyne, U.K.
[3]School of Engineering, Newcastle University, NE1 7RU Newcastle upon Tyne, U.K.
[4]School of Engineering, Nile University, Giza 3247010, Egypt
[5]School of Computing and Engineering, University of West London, W5 5RF London, U.K.
[6]Department of Brain Sciences, Faculty of Medicine, Imperial College London, SW7 2AZ London, U.K.

Corresponding authors: Xiaohan Sun (xhsun@seu.edu.cn) and Patrick Degenaar (patrick.degenaar@newcastle.ac.uk)

This work was supported in part by the Fundamental Research Funds for the Central Universities of China under Grant 2242022k30023, in part by Nanjing International Joint Research Project of China under Grant 202201017, in part by the Wellcome Trust under Grant 102037/Z/13/Z, in part by the Seventh Framework Programme under Grant 24986, and in part by the Engineering and Physical Sciences Research Council under Grant NS/A000026/1.

This work involved human subjects or animals in its research. Approval of all ethical and experimental procedures and protocols was granted by the Administration of the Animals in Science Regulation Unit of the Home Office, U.K.

ABSTRACT Optogenetic-based neuroprosthetic therapies are increasingly being considered for human trials. However, the optoelectronic design of clinical-grade optogenetic-based neuroprosthetic probes still requires some thought. Design constraints include light penetration into the brain, stimulation efficacy, and probe/tissue heating. Optimisation can be achieved through experimental iteration. However, this is costly, time-consuming and ethically problematic. Hence it is highly desirable to have an alternative to excessive animal trials. Thus, a simulation tool for optimising probe design can be an important benefit for the community. The challenge is to understand the interplay between the optical, neural and thermal aspects in the interaction of probe and living neural tissue. In this work, we propose a model which combines these aspects to allow clinically orientated neuroprosthetic teams to design neuroprosthetic probes for optogenetic therapies. Our model provides analyses for optical, thermal and optogenetic electrophysiological processes based on the energy equivalence and exchange among different physical fields. To validate and calibrate the model, optogenetic implantable neuroprosthetic arrayed probes based on miniature LEDs were developed. Then, optical, thermal measurement and neural photocurrent recording experiments were implemented on the probes. We can then provide analysis on exemplar arrayed neural probes.

INDEX TERMS Optogenetics, prosthetic brain implants, multi-physical fields coupling model, tissue optics, bioheat transfer, opto-neuro interaction.

I. INTRODUCTION

The field of implantable bioelectronics is steadily increasing. Applications include sensory neuroprosthetics, spinal, heart, and brain pacemakers, peripheral nerve bioelectronic medicine, and motor bionics. Underpinning the medical space is a requirement for advanced neural interfaces. Optogenetics [1] – the genetic photosensitization of neural tissue is an important tool for stimulating neural tissue. It has been used in human trials since 2015 [2], with the first

The associate editor coordinating the review of this manuscript and approving it for publication was Yogendra Kumar Prajapati.

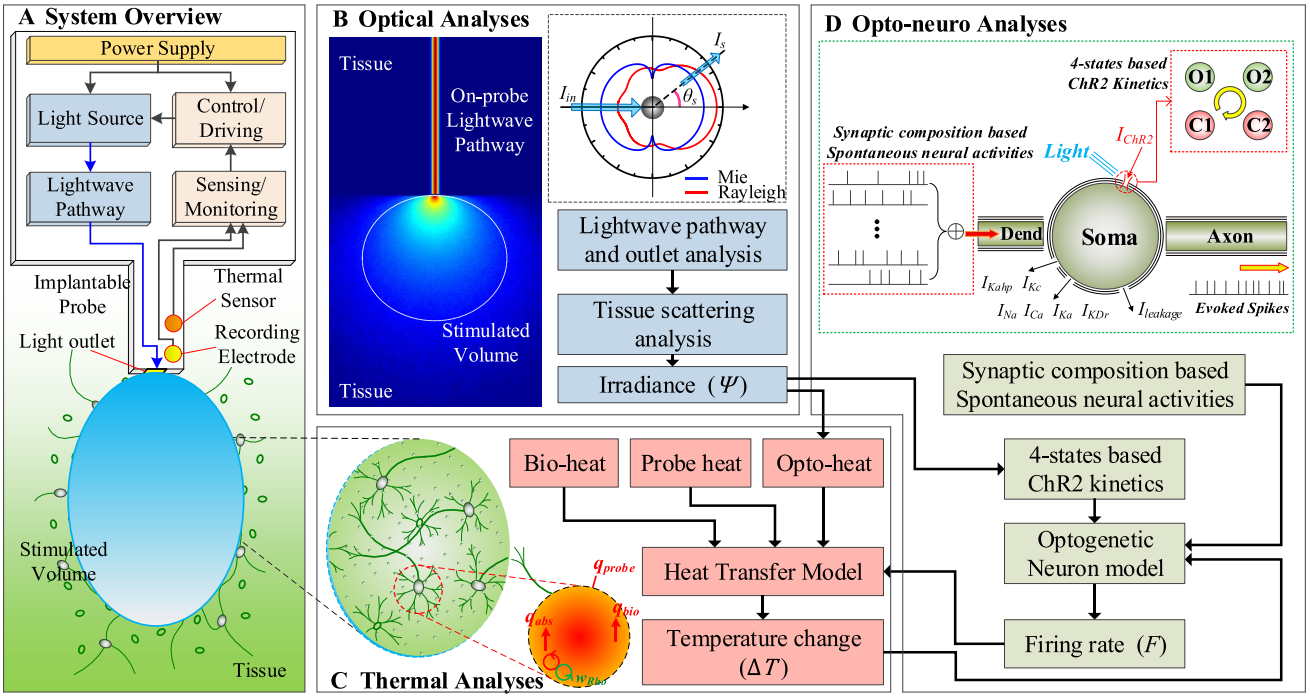

FIGURE 1. The schematic illustration of the OMFC model. (A) The overview of an implantable optogenetic neuroprosthetic system; (B) Optical analyses for Lightwave propagation and light diffusion in the tissue, the phase function of Mie and Rayleigh scattering in the tissue, from which the irradiance distribution is obtained to generate the opto-heat in (C) and supply the ChR2 kinetics in (D); (C) Thermal analyses for heat produced by probe, opto-tissue absorption and associated bio-heat, respectively, to obtain temperature change distribution ΔT by the heat transfer model within the simulated volume of the tissue; (D) Opto-neuro analyses, incorporating the ChR2 kinetics and spontaneous neural activities to form a modified neuron model so that firing rate distribution can be obtained as a final result.

results having been published recently [3] for retinal prosthetic applications [4], [5]. At the same time, closed-loop [6], [7] optogenetic solutions to the treatment of human focal epilepsy are at an earlier stage of exploration [8], [9]. These specific applications require the development of an optogenetic neuroprosthetic system and corresponding implantable probes.

Progress has been made in developing several prototypes of optogenetic implantable neuroprosthetic probes, from the early fibre-optic-based implants [10], to highly-compact μLED based non-invasive visual prosthesis [5], deep brain implants [11] and photonic-circuits based brain implants [12]. Each of these techniques has specific pros and cons. However, in all cases, there is a need to understand the stimulus profile for light emitted within a given thermal limit. This is particularly true for μLED based optrodes, as heat is generated close to the target neural tissue. These design constraints must be fully understood to optimise the probe architecture for a given clinical application.

Past efforts to explore the optical emission profile have included linear models such as Kulbelka-Munk [10], which provides some insight for collimated light. However, the emission functions of LEDs typically have Lambertian emission functions [5], and even optical fibers will emit dispersively. As, such, Azimipour and ourselves have explored Monte-Carlo approaches [13], [14], [15], and Yona et al. has explored numerical beam spread function approaches [16]. The second consideration is the thermal effect, due to either light absorption or heating effects from inefficiencies in the LEDs. Current standards for implantable medical devices state that the surface temperature of an implant should not exceed +2° C [13] above ambient. As such, the probe emission radiance will ultimately be limited by thermal effects due to inefficiencies photonic generation and coupling (as opposed to internal reflection). McAlinden et al. explored thermal-optical relationships for their probe [17], though they did not consider the fundamental heating of the tissue due to the absorbed light, as per Stujenske et al. [18]. Dubois et al. explored the issue further for optical fibres [19], and we did similarly for LED emissive probes [13]. Furthermore, we developed a method to use LEDs to measure their own temperature profile after being turned off [20], [21]. We could, therefore, explore temperature cycling in non-human primates.The third consideration is how the optical emission results in actual neural stimulation – i.e., increased (or decreased [22]) firing rates. We can use the 4-state photocycle model of channelrhodopsin-2 (ChR2) [23] to understand the optically induced current provided to neurons. This model has also been computationally integrated into a Hodgkin-Huxley neuron model to describe the cell-level optogenetics [24], [25], and, more recently, combined with meanfield theories or networking configurations to describe the mechanisms of more macroscopic optogenetic neuromodulation [26], [27]. However, up to now, such biophysical

analysis of neural operation has little cooperation with optical and thermal analysis to explore the effective stimulus potential of a given probe architecture. Though efforts have been made, e.g by Peixoto et al. [28], it lacks experimental validations and calibrations.

These three considerations could allow probe designers to explore the trade-offs between the optical, thermal and biophysical characteristics. Furthermore, it allows scientists to consider the effect of given design constraints on the therapeutic effects, whether open loop or closed loop [29], [30].

In this paper, we propose an optogenetic multiphysical fields coupling (OMFC) model for optimising and understanding the performance of implantable neuroprosthetic probes. We have validated and calibrated the model predictions with experimental data for each analysis. Then, using our validated model, we have explored implications for a standard concept optogenetic neuroprosthetic probe.

II. THE OMFC MODEL

A. SCHEME

Figure 1 shows the schematic illustration of the OMFC model. A practical implantable optogenetic neuroprosthetic system would conceptually have a power supply, light source, lightwave pathway (if using a light guide), control/driving, and sensing/monitoring capabilities. (figure 1A). The probe would then generate an optical stimulus at the required location in the tissue through light outlets or directly from the LED. Past examples of probes with optical waveguide structures include: [12], [31], [32].

Similarly, past examples of probes with embedded emitters (e.g. microLED) include: [13], [17]. The probe would typically have an electrical recording system and potentially thermal monitoring. The response of neural tissue to the probe should consider the parameters that could consist of the distribution of irradiance, temperature profiles, and resultant firing rate.

The simulation space can be defined as three volumes: The overall simulation volume V, the space consumed by the probe, and the stimulation volume V_s. We define this latter volume as the domain where the optical irradiance exceeds the response threshold. The OMFC model can then be established by interrelating the three primary design constraints.

The optical properties of tissue are usually characterized by light scattering and absorption, both of which occur from the complex physical and biochemical structure of tissue. Light diffuses in the tissue due to scattering and absorption, and the absorption is the result of a large number of molecules and proteins [33]. Therefore, the total absorption can be seen as a combination of ChR2 and intrinsic tissue absorption. The intrinsic absorption of the cortex at 450-500nm is about 0.1-0.2cm^{-1}, while it rises to above 1 cm^{-1} for astrocytes of nerves, according to the previous publications [34], [35].

ChR2 has considerable absorption at its sensitive wavelength, which was reported to be up to 50000 M^{-1}cm^{-1} [36], but it only exists as an ultra-thin layer on the cell membrane, and depends on expression levels. However, while brain tissue scatters blue light very strongly, the absorption coefficient is small $\sim$1cm^{-1}. As such, given that the light will eventually be absorbed by either the ChR2 or other aspects of the tissue, we cautiously estimate this ratio to be in the range of 30-70% depending on the ChR2 expression level and the proportion of cells which are expressing it [37], [38]. The rest of the light absorption will be from other aspects of the tissue.

Wild-type ChR2 therefore requires a photon flux of 10^{15}-10^{17} photons/mm$^2\cdot$ s (0.4-40 mW/mm^2) to be reliably activated [39]. As such, for reliable activation of action potentials in dissociated neurons, a 5ms pulse of 1 mW/mm^2 is considered to be the threshold [24], [40].

It should also be noted that the majority of the light will also disperse beyond the stimulation region. For simplicity, we assume homogeneous expression at a defined level. The scattering aspects of the model are presented in Figure 1B.

Absorption of a photon by ChR2 activates its photo-induced isomerization cycle, while the intrinsic tissue absorption converts to heat. The ChR2 photocycle also ultimately contributes to heat. Optical heating will, therefore be in tandem with any direct heating from the probe, and the active environment in the tissue, as per Figure 1C.

The photon absorption in ChR2 causes it to transit into an excited state within the period of $\sim 10^{-6}$s. In turn, that causes the channel to open, resulting in ion flow (I_{ChR2}) into the cell [37]. ChR2 can be modelled to have light and dark-adapted photocycles with different open-state efficiencies [23], [24], [25], [41]. As the ChR2 relaxes to the ground state, the photonic energy will transfer to thermal energy in the tissue. The ChR2 activity is integrated as an ion channel in the Hodgkin-Huxley model of the neuron as per Figure 1D.

B. MODELLING THEORY

Assuming the total power injected into the tissue is P_0, the primary energy equivalence relation of the system can be written as

$$P_0 - \oiint_{\partial V} \boldsymbol{\phi_{em}} \cdot \boldsymbol{ds} = \iiint_V q_{probe} dv + \iiint_V q_{abs} dv \quad (1)$$

where ∂V is the closed surface of arbitrary volume V surrounding the implantable probe in the tissue, $\boldsymbol{\phi_{em}}$ is the electromagnetic energy-flux density, which can be solved in the optical analysis. The second term on the left side ($\oiint_{\partial V} \phi_{em} ds$) represents the output flow of the electromagnetic power through ∂V. Both sides of the equation represent the power increase within volume V. The first and second terms on the right side represent loss-induced heat in the probe and opto-heat caused by opto-tissue absorption, respectively.

Then, we define the response function $\mathbb{R}$ to quantify the performance of the implantable optogenetic neuroprosthetic system:

$$\mathbb{R} = \{\Psi(X, P_0), \Delta T(\Psi, X, F, T), F(\Psi, X, T)\} \quad (2)$$

where Ψ, ΔT and F represent the distribution of irradiance, temperature change, and evoked firing rate in the tissue, respectively, while X is a series of design variables for probe structure, and T is the temperature. ΔT and F are both related to Ψ and related to each other, and $\Psi \propto |\boldsymbol{\phi}_{em}|$. This allows us to implement inverse design to the optogenetic neuroprosthetic system by setting objectives and constraints to find proper design variables.

The optical analyses in the OMFC model follows the framework in our previous work [13]. The pattern of optical stimulus was obtained by analyzing the lightwave pathway and the subsequent emission from the outlet of a given probe, based on the wave theory of optics [42], [43]. Meanwhile, light scattering in the tissue was solved by a combined Mie-Rayleigh scattering and absorption theory [44], [45]. As such, the irradiance distribution Ψ of the diffused light in the stimulation volume V_s could be obtained through a Monte-Carlo light transportation method [46].

In the thermal analyses, the majority of the heat generated in the V_s (highlighted by yellow) was considered to come from three sources: heat from light absorption (q_{abs}), biomedical metabolism (q_{bio}), and considerable Joule heat conducted from the probe (q_{probe}), respectively. Part of the absorbed optical energy (w_{Rho}) was stored in the ChR2 to trigger the ChR2 photocycle, and was relaxed to contribute to the thermal fluctuation. It should be noted that the ChR2 comprises only a tiny proportion of the total tissue volume – the cell membrane. The absorption of ChR2 is transient ($\sim 10^{-6}$ s), and its thermal contribution lasts during the whole photocycle. Metabolism is usually known as the thermal base of the tissue. It is reported to be a much slower source of the order of magnitude of 0.01 mW/mm^3 for the brain cortex [47]. Considering convection through blood vessels as in Penne's model [48], we think metabolism is a minor factor and is normally in equilibrium. By integrating in the full V_s, the temperature change distribution (ΔT) could be obtained. On-probe heat transfer was solved by a time-resolved heat equation [49]. Heat transfer in the brain tissue was solved by modifying Pennes' model of bio-heat transfer to include the optical absorption effect [48].

In the opto-neuro analyses, the expected distribution of firing rates F in the tissue is solved from the distribution of irradiance. As the real firing rate is also determined by the morphology and spatial distribution of the neurons, etc., assumptions were made here to consider the ChR2-intermediated optogenetic neurons are uniformly distributed, and the crosstalk among the neurons are neglected. The cell-level response was described by the ChR2-CA3 model, which combined the ChR2 ion channel kinetics to the Hodgkin-Huxley type CA3-cell neuron model [23], [24]. Each neuron model has synaptic input based on Poisson spiking events train following specific neural oscillation waveform. The ChR2 kinetics are based on a four-state transition rate model (the states are two closed and two open, C1, C2, O1 and O2 states) [41]. The neuron model incorporates wild-type ion channels, including the voltage-dependent ion channels (I_{Na} I_{Ca}, I_{KDr}, I_{Ka}), calcium-dependent ion channels (I_{Kahp}, I_{Kc}) and leakage channel (I_{leak}) [24]. The analyses have the capacity to update the parameters to mimic detailed bio-realistic conditions if required.

The optical analyses in our model were done by a custom-coded program with Matlab 2020b (Mathworks inc.). The thermal analyses in our model were built in COMSOL Multiphysics (COMSOL inc.). The neural analyses in our model were done by custom-coded program with Matlab 2020b (Mathworks inc.).

III. SIMULATION AND ANALYSES

A. THERMAL CONSTRAINT AND HOT SPOT ANALYSIS

The long term effects of transient and even sustained temperature rises of a few degrees is actually not known. Prior work has shown the sensitivity of firing rates to temperature [50], [51]. Other works have provided a theoretical basis for how temperature can change the firing rate [28], [52], [53], but given that the objective of the optogenetic stimulus is to modulate neuronal behavior, that in itself is not necessarily problematic.

In previous work, we provided the regulatory constraint that the temperature of any implant surface should not exceed 2°C as per [54]. However, it should be noted that a transient temperature rise from a high heat capacity material imparts much more thermal impact than the equivalent rise from a material of low heat capacity. As such, a temperature rise of a few degrees on a microscale probe will not have the same impact on the tissue as a few degrees of temperature rise from e.g. a large heart pacemaker control unit.

In order to properly assess the thermal impact of the probe, we compare two aspects: (1) the probe surface hot spot above the LED (ΔT_P) resulting from thermal generation from the LED resulting in a transient surface temperature (2) the in-tissue hot spot (ΔT_t) at the depths of 25, 50μm, resulting from the induced heat from the probe, optical absorption, and passive/active thermal extraction from the tissue.

The efficiency of on-probe mini and micro-LEDs vary in the literature. Generally, micro LEDs such as that previously reviewed by ourselves [13] have low efficiencies of 1-5%. But commercially available mini LEDs have efficiencies of the order of 20- 40%. There are many reasons for this, including processing defects, the quality of materials available to academic labs, and the ratio of surface defects to bulk. This will improve in time, but we can assume practical probes have efficiencies in the range of 1-40%.

Table 1 shows the results of the hot spot analysis. Given the demanded radiance density of the emitter is 100 mW/mm^2, heat power generated on-probe widely ranged from 11.5 to 760 mW for different LED efficiencies (1%, 10%, 40%). The temperature change of the on-probe hot spot ΔT_P were obtained for different pulse duration (10 ms, 50 ms). Meanwhile, the in-tissue hot spot ΔT_t was obtained by calculating the temperature change within a miniature voxel ($\sim 1000\mu$m^3) close to the probe-tissue interface. We set the

TABLE 1. Hot spot analysis for different heat sources.

Efficiency (%)	Pulse duration (ms)	ΔT_P (°C)	ΔT_t (°C) 25μm depths	50μm depths
1	10	3.03	2.14	1.73
1	50	34	25.5	21.4
10	10	0.29	0.19	0.14
10	50	3.32	2.38	1.93
40	10	0.2	0.12	0.09
40	50	0.7	0.43	0.36

intrinsic tissue absorption coefficient to be 1 cm^{-1}, so the corresponding absorption-induced heat is about 20mW/mm^3 within a very small distance ($\sim 10\mu$m) close to the LED emitter when the stimulation is on.

At 10% efficiency for the LED, the thermal contribution of light absorption is only 1/5 of the Joule heating at most, and decays rapidly with depth in the tissue. It reduces to 18 and 14 respectively at 25 and 50μm to the probe. The thermal contribution of metabolism is even 1-2 orders of magnitude less. The heat power on-probe rapidly decreases when the efficiency increases. At 40% efficiency, the two hot spots are comparable.

A common arrangement for cortical implants is for a fork shaped design as per Figure 2 or an array thereof. We, therefore want to use the OMFC model to draw some conclusions as to the scalability of this design.

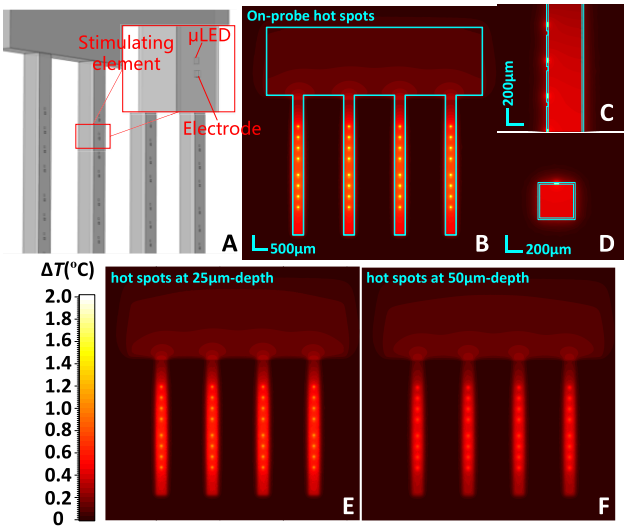

FIGURE 2. Fork-shaped arrayed implantable probes with GaN μLEDs: (A) illustration of the stimulating elements; (B) Distribution profile of the temperature change (ΔT), top view at the surface of the probes; (C) thermal profile, side-view along one probe; (D) thermal profile, cross-section view of one probe; (E) top view thermal profile at 25μm-depth from the probes; (F) top view thermal profile at 50μm-depth from the probes.

We used the structure in Figure 2. probe length is 5.5 mm long and 2 mm in spacing with each other. As shown in Figure 2(A), each probe has 8 stimulating elements consisting of a GaN μLED and a bare, tissue-contacting electrode for recording. The distance between adjacent stimulating elements is 422.5μm. We chose these dimensions as potentially clinically useful given the pre-clinical CANDO project being developed at Newcastle University [13], [30]. We defined the LEDs as relatively punctate emitters of dimension 50 × 50μm. The emitting characteristics of the LEDs could be both Lambertian, and optical shaped, while the later has a better-collimated profile in the output beam. Here we take an exemplar μLED quantum efficiency of 10%, given that practical LED efficiencies can range from 40% to less than 1%. We also determined the thermal constraint. $T_c = 2°C$ at the probe surface as per regulatory requirement [13]. Though it should be noted that we feel this is very conservative, given the expected impact on the tissue is significantly lower as per Table 1. Figure 2 (B) to (F) show the thermal profile with hot spots, for the fork-shaped probes at different viewpoints. Under the stimulating protocol of short pulses (<50ms) and proper duty ratio (<0.4), primary hot spots could be localized near the LED emitting surface, while secondary hot spots were generated around the recording electrodes. As per above, light absorption contributes to non-negligible thermal effects in the tissue. However as per Table 1, the overall effect is typically that the expected temperature rise in the tissue is lower than for the probe surface. We can therefore use the maximum temperature rise to determine the maximum emitter power.

As such, the ΔT of the primary hot spots can reach the thermal limit of 2°C (Figure 2 (B)). But it reduces rapidly with depth into the tissue from the probe, to ~1.3°C at a depth of 25μm (Figure 2(E)), and ~0.7°C at a depth of 50μm (Figure 2(F)). It should also be noted that we can expect a gliosis layer to form around the probe within this range.

B. MAPPING THE RESPONSE OF THE NEURAL TISSUE

In practice, neurons at different locations in the tissue will be activated at different firing rates because of different local irradiance, absorption as well as temperature change ΔT. Especially for accurate optogenetics with cellular and subcellular spatial resolution, the cross-section of the stimulating pattern could be as low as several micrometers. Miniature light-emitting sources or advanced collimated beam technologies are usually implemented to reach such required resolution. This could be quantitatively analyzed in our OMFC model.

Figure 3(A) shows an example by using an implantable probe embedded with micro-LED (μLED). Neurons at different depths in the tissue were stimulated, while the gliosis region and a thermal limit region were also shown. The degradation region indicates the volume where no spikes could be evoked after implantation as per above. The thermal limit region indicates the volume where ΔT (of the probe surface) may exceed the thermal limit of 2°C. As such, after implantation, neurons could only be effectively stimulated when they were included neither in the gliosis region nor in the thermal limit region. From the discussion as per above, ΔT reduces by 40-60% within the gliosis region

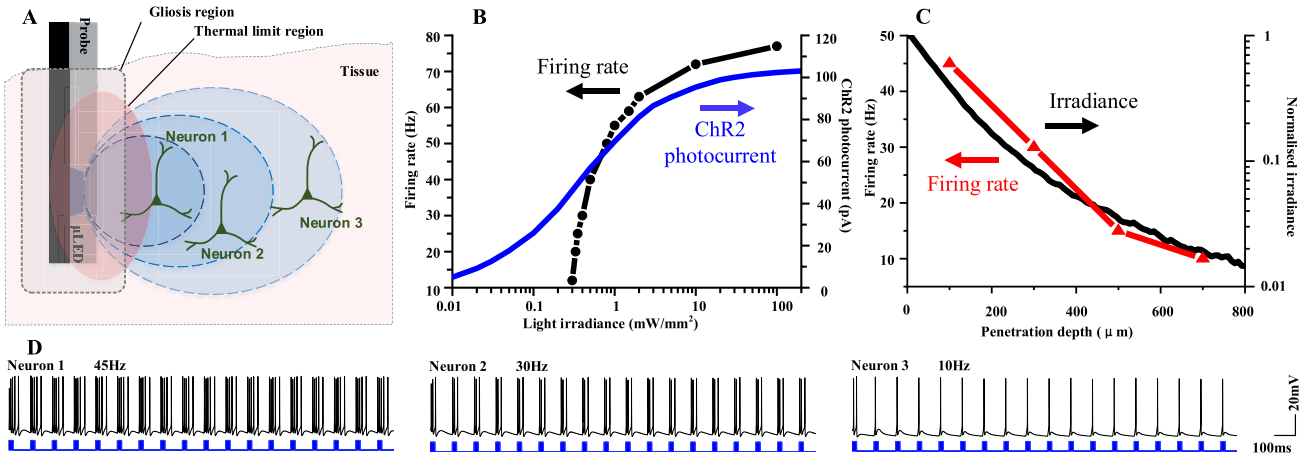

FIGURE 3. Response map of the neural tissue: (A) Diagram of the response map for an implantable probe. (B) Response range of the ChR2 photocurrent and corresponding firing rate with respect to light irradiance. (C) Expected light-induced firing rate with respect to the penetration depth of light. (D) simulated results of the light-induced spikes for neuron 1, 2 and 3 at different depths to the probe.

(∼50μm). ChR2 photocurrent and light-induced firing spikes evoked by 10 Hz pulse train at a wide range of local irradiance (0.01 to 100mW/mm2) were calculated according to the model. As shown in Figure 3(B) shows results according to model prediction: The ChR2 photocurrent ranges from 5-105pA, and the corresponding firing rate excited at the neuron is 10-80Hz with a threshold irradiance about 0.5 mW/mm2. Combined optical and opto-neuro analyses, Figure 3(C) shows the expected light-induced firing rate (red line), in relation to the penetration depth of light in the tissue. The simulated firing rate reduces from about 45Hz to 10Hz while the depth increases from 100 to 700 μm to the μLED. Corresponding irradiance (black line) were also shown in Figure 3(C). Figure 3(D) shows the waveform of the spikes for three neurons at different depth. The neuron can fire spike trains at a phase-locked rate of about 10 Hz (Neuron 3, Figure 3(D) right panel). For fairly high irradiance of 10 mW/mm2 the neuron can fire spike clusters at the phase-locked rate (Neuron 2, Figure 3(D) middle panel), while the spike number in one group increases from 3-4 to 5-7 when the irradiance increase to 100 mW/mm2 (Neuron 1, Figure 3(D) left panel).

As different irradiance results in different firing rates, the response function $\mathbb{R}$ in equation (2) of a given probe could be obtained and mapped in the tissue. Thus, the optimal performance of the probe can be quantified. Following that, the radiance distribution of light emitted from the probes can be attained.

IV. EXPERIMENTS

The OMFC model incorporating models of multiple physical fields, and it could be preliminarily validated and calibrated by measuring some key output quantities (Ψ, F, ΔT), according to equation (2). The experimental validations were performed with test probes based on mini-LEDs emitting 470nm light. Both single-shafted probe and fork-shaped arrayed probes with multiple shafts were developed for the experiments.

A. VALIDATION AND CALIBRATION OF THE OPTICAL AND OPTO-NEURO ANALYSES

1) EXPERIMENTS SETUP

The validation of the optical analyses was through light penetration and scattering experiments in brain slices extracted from 6-week old C57BL6 mice, on the basis of our previous work [13]. light penetration and scattering in slices with different thicknesses (50-500μm) were measured with an 14bits Andor iXon DV887 back-illuminated EMCCD camera through Olympus microscope lens system (Olympus 2.5X NA).

The firing rate F could be determined by the dynamics of transmembrane current in the opto-neuro analyses, so we performed ChR2 photocurrent recording experiments on ChR2-transfected neurons, in order to validate the opto-neuro analyses and calibrate the irradiance in the tissue obtained in the optical experiments.

Figure 4(A) shows the setup of the ChR2 photocurrent recording experiments, which can be also used in the light penetration and scattering experiments without the voltage clamp system. In the experiments, the neuron cells were extracted from the tissue and patched on the tissue surface. In this way, we could use the cells as mobile light sensors. Photocurrents of cells at different depths of the tissue while separately illuminating from above using the microscope LED illuminator and from below through the tissue by the mini-LED test probe. This was to compare relative responses with the calibrated microscope illumination, as Figure 4(B) shows. The test probe based on mini-LED (CREE DA2432) was fabricated from silicon with evaporated metal strips, and the LED was bonded using a Fineplacer bonding tool. The probe was then coated in parylene for encapsulation. The probe can be seen in Figure 4(C).

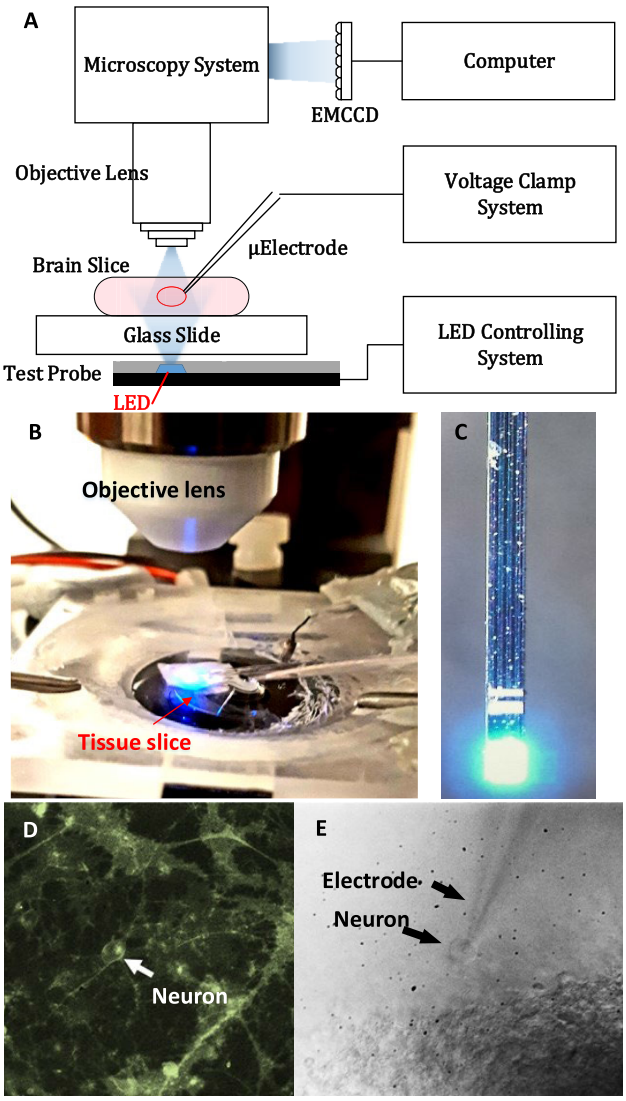

FIGURE 4. (A) Experiments setup; (B) Photograph of the experimetns; (C) A single-shafted probe based on miniLED; (D) Photograph of an example dissociated neuron (highlighted by white arrows) with the co-expression of EYFP marker; (E) DIC image of the example neuron in the nucleated-patch configuration for whole-cell recording.

The experiments were implemented with transgenic mice expressing ChR2 under the Emx1 promoter (Jackson Laboratory, Maine, USA), which gives strong labelling in all forebrain-generated cells, including pyramidal neurons but excluding interneurons. Mice with widespread, stable and reliable ChR2 expression were sacrificed by cervical dislocation, and brains were immediately transferred to ice-cold oxygenated artificial cerebrospinal fluid (ACSF). Brain slices of different thicknesses (300 and 500μm) were prepared and then transferred to a submerged incubation chamber containing ACSF, for a minimum of 1 hour prior to recording. Continuously perfused with oxygenated ACSF (room temperature), cells in the brain slices were recorded in whole-cell patch-clamp mode. Patch-pipettes (resistance 5-7 MΩ) were made from borosilicate glass capillary tubes (0.86mm internal diameter; Harvard Apparatus, Cambridge, UK) using an electrode puller (P-87; Sutter Instrument Co, CA, USA). Patch-pipettes were filled with artificial intracellular solution (K-methyl-SO_4 125mM, Hepes 10mM, Mg-ATP 2.5mM, NaCl 6mM). Both the microscope objective and headstage positioning were controlled by individual micromanipulators (Patch star PS-700C; Scientifica, East Sussex, UK), enabling precise movements over three orthotropic axes. To reduce electrical noise, all apparatus was placed in a Faraday cage, and the electrical items were individually grounded to earth. Patch-clamp recordings were made using an Axopatch 700B amplifier/Digidata 1440A interface (Axon Instruments; Foster City, CA, USA) controlled by Clampex 10.5 software. Signals were sampled at 10 kHz and low-pass filtered at 2 kHz.

Brain slices were placed on top of the test probe. This configuration enabled illumination of the tissue from underneath using the probe LED or from above using the microscope LED illumination (465nm; COOL LED pE system). After achieving whole-cell recording mode and verifying that the cell expressed opsin through a test illumination, a ''nucleated patch'' was pulled. This technique creates a large, outside-out patch, containing the nucleus of the cell, which displays macroscopic currents, and, importantly, also allows one to move the patch electrode. The nucleated patch could thus be relocated precisely above the CREE-LED, and separated by tissue of a specified width.

2) VALIDATION AND CALIBRATION RESULTS

The profile of the diffused light in the tissue is generally determined by the scattering, which occurs whenever light encounters a refractive index change. The scattering properties of the neural tissue are determined by the spatial variations in refractive index at the operating wavelength. The exact description of refractive index distribution in the tissue is not feasible to know, for it is determined by the exact spatial distribution of the cellular and subcellular structures [33]. Therefore, statistic descriptions could be implemented. In this way, the tissue could be seen as a mess of scattering particles with fractionally distributed sizes, as we reported in our previous work [13]. Refractive indices were taken from the previous publications, e.g. cortical cytoplasm (1.353 to 1.368), protein (1.5), lipid (1.48), etc [33].

The probe implantation can typically create a small region of degradation around the insertion site. This can be caused due to migration of micro-glia cells in response to the probe insertion. Such effects can occur over days to weeks post-implantation, but eventually, we need to assume that the emitted light needs to traverse a minimum distance beyond this region to have a therapeutic effect. Therefore, we have assumed the degraded tissue region to be at a depth of up to 50μm from the probe surface.

Previous research indicated that photocurrent reaches to a peak value under abundant illumination, and with the duration of illumination, it degrades to a lower and steadier plateau state [23]. This is attributed to the shift from dark-adapted to light-adapted states in the ChR2 and depletion of ground-state

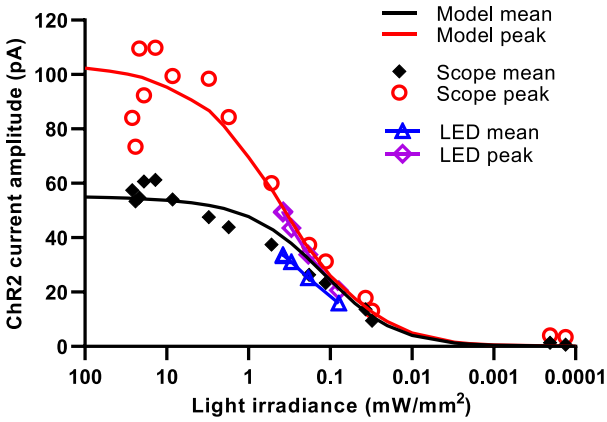

FIGURE 5. Opto-neuro analyses validation: ChR2 current amplitude in relation to the light irradiance, both mean and peak value of the scope illumination and probe LED illumination from the test probe were compared to the simulation results.

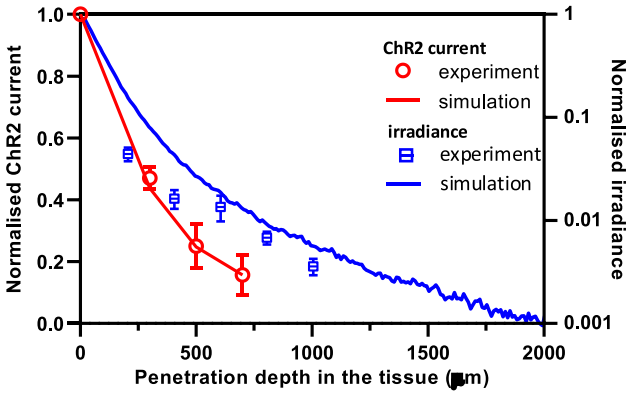

FIGURE 6. Opto-neuro analyses validation: (right y-axis) normalized irradiance attenuation along the penetration depth, and (left y-axis) normalized ChR2 current in relation to penetration depth in the tissue.

opsins [41]. Figure 5 shows the dependence of ChR2 current amplitude on light irradiance for both peak and mean values with the plateau. Microscope illumination was implemented to obtain a reference ChR2 current (red and black symbols) in a broad range of light irradiance for both peak and mean values with the plateau from 10^{-4} to 100 mW/mm^2 on the tissue surface. The model predictions of both peak and mean values (red and black lines) were obtained by applying the OMFC model to the probe LED and the tissue slice. As the irradiance distribution in the slice could be obtained in the optical analyses, the ChR2 current and evoked spike rates in anywhere of the tissue slice could be derived through the opto-neuro analyses from the irradiance distribution. As shown in Figure 5, the model prediction of the ChR2 current is very similar to the reference value. Restricted by the LED irradiance (about 0.1-1mW/mm^2), the recorded photocurrent by the probe LED was within the range of 10-50pA (blue and purple symbol lines), and it is coincident with the reference and model prediction.

In the experiments, we used the patched cells as mobile light sensors to obtain the photocurrent at different depths of the tissue. In the simulation, we calculated the profile of the light diffusion in advance, then the induced photocurrent at 0, 300, 500 and 700μm depths were obtained through the opto-neuro analyses. As so, the optical and opto-neuro analyses could be validated by comparing the simulation and experiment results of the depth-dependent ChR2 current and irradiance in the tissue. Such comparisons are shown in Figure 6.

The measured irradiance is shown with blue symbols in Figure 6, to compare with the simulated results (blue line). We compared the simulated and measured results by normalising the irradiances of transverse patterns through different thicknesses (200 to 1000μm). It shows that the attenuation of irradiance along the penetrating depth in the tissue basically have the same curve for both simulated and measured results, the simulated irradiance is about 20% higher than the measured one within the first 1mm, and this difference narrows with deeper depth. It looks the simulation is becoming more inaccurate as the tissue gets thinner. Specifically, the intensity is less than expected. We think this is most likely due to a surface scattering and/or reflection effect that we haven't taken into account in the model. Other factors like the improvement of detailed refractive index distribution, e.g. the refractive index variations of layer 1-4 cortical tissue, scattering particles, etc. could also be considered [55]. Despite the above imperfections in fitting, we believe that as the distance increases, the simulation will converge with the actual situation.

Figure 6 also shows the validated results of normalized ChR2 current through ChR2 current recording experiments. In the experiments, we used the patched cells as mobile light sensors to obtain the photocurrent at different depths of the tissue. In the simulation, we calculated the profile of the light diffusion in advance, and then the induced photocurrent at 0, 300, 500 and 700μm depths were obtained through the opto-neuro analyses. Both experimental and simulated photocurrent have been normalized to the value at a depth of 0μm. Measured currents under different LED driving powers (red symbols in Figure 6, with the LED irradiance from 1-5mW/mm^2) were normalized to shows the depth dependence. Simulation results under the same conditions were shown in black symbol-line for comparison. The comparison results show that the experimental and simulated ChR2 current keeps the same descent along the light penetration depth in the tissue. Thus, we trust the ability of opto-neuro analyses to obtain the expected firing rates of a given optogenetic neuroprosthetic system. This also helps show the calibration of the irradiance in the tissue.

B. VALIDATION AND CALIBRATION OF THE THERNAL ANALYSES

In the OMFC model, heat in the tissue consists of three parts: heat from light absorption (q_{abs}), biomedical metabolism (q_{bio}), and considerable Joule heat conducted from the probe (q_{probe}), respectively. Direct measurement of local temperature and thus, thermal heating in fluid/tissue is very challenging. In previous work we found a way to utilize the

probe as its own temperature sensor, but even in this case, careful calibration is required [21]. As such, for this study, as per previous work, we implemented thermal measurement experiments by utilizing thermal imaging in air to monitor the surface temperature profile of test probes. This could then be used to calibrate our model from which to make predictions in tissue [13]. In the experiments, Fork-shaped test probes with multiple shafts were developed by mounting a Gallium Nitride (GaN) mini LED (CREE DA2432) onto the silicon base. The dimension for each shaft is $5\times0.3\times0.2$mm. The LED was set near the end of each shaft and connected to the wire-bonded connectors through Titanium-gold lines. For experimentation, the LED was powered by an isolated pulse stimulator (2100, A-M SYSTEMS, Hinckley, UK); enabling control of the amplitude, frequency and duration of the current. Thermal measurements of the probe surface temperature in the air were taken with an Optris microbolometer IR camera, and the captured image is displayed in a digital imaging system.

Figure 7 shows the validation and calibration of thermal analyses through thermal measurement experiments, and ΔT was defined as the surface temperature change of the hot spot on the probe. The thermal image as per Figure 7(A), is a mixture of black body radiation from the source and reflected thermal signals from the surrounding area. The ratio of the two is defined as the emissivity (where 1 is an ideal black body, and 0 is a perfect mirror). The emissivity of our silicon probes is low, so we calibrated them according to the difference in temperature from a reference temperature point (26°C). Two hot spots were captured where the LEDs were turned on. The key heat source results from the LEDs, though it should be noted for active electronic probes (e.g. Neuropixels probes [56]), there will also be a fixed head source in the base of the probes. The LEDs were driven with a wide power range up to 121mW, with an optical conversion efficiency of about 30%. The heating process persisted for about 120s, and our imaging system recorded the temperature change of every 10ms.

Figure 7(B) shows both measured and simulated ΔT at hot spot 2 in 300 seconds (covering a full heating process), under the driving power of 45.6, 64.6 and 86.5mW. Although there are limited differences in the range of 10ms to 1s, and beyond 120s, this comparison shows a general coincidence in the specific time-dependent ΔT between the simulation and measurements, for they reached the same maximum temperature and cooled down in the same time dimensions. As such, we basically did our calibration for the model in air, and we then translated it to the model in the tissue/fluid. An important parameter we could obtain from the calibration is the driving power of the LEDs under a certain thermal constraint. Though there could be some parameter errors in that translation, we believed it to be still valid. Figure 7(C) shows the ΔT with respect to the LED driving power, for heating time widely ranged from 20ms to 1s. The symbols are measured values, while the lines are the simulation results from the calibrated model.

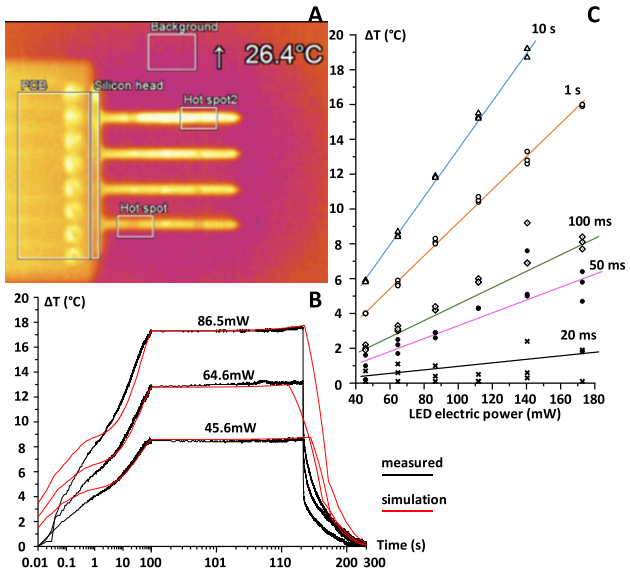

FIGURE 7. Thermal analyses validation: (A) Fork-shaped arrayed test probes under temperature measurement (top view); (B) Time-dependent temperature change of the probe for different heat power for 45.6 – 86.5mW LED are compared with simulation (red line); (C) Calibrated temperature change with respect to the LED driving power, for different heating time.

In using the thermal analyses, a major limitation is that the thermal decay for the measurements is substantially faster than the model in Figure 7(B). This would bring errors in determining the duty cycle of a pulse train, given many neuromodulating strategies use them.

V. DISCUSSION

When considering the light emitted by a collimated laser, the intensity will rapidly decay with distance as an exponential with the extinction coefficient. Extinction being the combination of absorption and scattering. However, if we consider the 3D emission profile, the situation is more complex. Scattered light is not lost, it is simply deflected. Eventually, the light will be absorbed by the tissue, but its irradiance profile is largely dependent on its dispersion through the tissue by scattering. The scattering is also anisotropic, such that around 90% of the light is scattered in a forward arc and 10% is scattered back.

If the initial light emission is collimated, then the dispersion profile will be different than if the emitter was Lambertian (emitting as a spherical profile from the emitter). As such, we assumed a Lambertian profile of emittance from our LEDs, as this is typical in air. However, the refractive index of tissue is greater than in air. So, the profile could be different. We unfortunately did not have the tools to measure the illumination profile of the LED in water. As such, taking the irradiance profile along a linear perpendicular line from the emitter center will be slightly different from our model and what we measured in Figures 3, 5.

There is some discussion in the field about the appropriate measure for maximum temperature. The regulations state that the probe surface temperature should not exceed +2 °C. Our

simulations indicate that with that limit, tissue hot spots will have declined to less than $+1°C$ within $50\mu m$ of the surface. As we expect this region to be effectively dead, then a probe surface temperature limit of $+2°C$ is unlikely to cause further damage to the neural tissue.

Our enucleated neuron experiments allowed for interesting studies of the direct effect of light on the inward current into the neuron. This could be connected with the well-known channel dynamics of ChR2, and thus explore the effect of tissue thickness on the scattering profile of light from an LED-based probe. However, there are two caveats to this work: (i) We did not directly explore light vs firing rate for our neuron (ii) there are many neuron types in the body, and our original model [23], [24] for the opto-neuron was from hippocampal cells. As such, the model parameters would need to be updated for the cells of interest – e.g. cortical pyramidal or interneurons.

Furthermore, we take a punctate approach, providing the equivalent frequency if a neuron soma was embedded at a given depth from the probe. This is clearly a simplification from the 3D structure of individual neurons, and their 3D structure. Furthermore, neurons talk to each other in a network. So there would be an additional layer of complexity required to directly connect a probe design with specific peturbations to particular neural circuits. But the purpose of this work is to determine an optimal probe design. A 3D map of expected current injection stimulus can be created from this and transferred to such neuron network models if required. Our neuron model is able to predict the firing rate from ChR2 photocurrent. Considering spontaneous neural activities. As such, we can generate a map of firing rate, once we know the spatial distribution of the neuronal compartments in the tissue.

Direct measurement of local temperature and thus, thermal heating in fluid/tissue is very challenging. We previously developed a tool to achieve this with the probes themselves, but the actual measurement is at the p-n junction of the diode rather than the surface. So it relies on a model to provide a result, and we felt this to be circular for this work. Infrared microscopy can be used to look at temperature distributions in air, but not through water. As such, we had to do our calibration for a model in air and then translate that to our tissue/fluid model. As such, there could be some parameter errors in that translation, though we believe it to be still very valid.

Combining our analyses, we were able to create, for the first time, a map of the response function, including the distribution of irradiance, temperature change and the evoked firing rate for an optogenetic implantable neuroprosthetic probe. We envisage this tool allowing future teams to evaluate probe design trade-offs prior to expensive rounds of design and challenging testing.

In general, the OMFC model is still a simplified model. Our advantages include an integrated analysis relating different physical fields involved. Parameters in our model have been calibrated experimentally, so we think the model does have some basis in real biophysics. The limitations of the model include over-simplification of the morphology and interconnected networks of neurons, and will be improved in the future work.

By configuring the thermal constraint to a safe value, we neglected the discussion on opto-thermal sensitivities of neural activities. We also did not include consideration of neuronal interconnections as we believe this should be thoroughly investigated in a separate paper.

For now, our model focuses on the 470 nm light and channelrhodopsin-2 (ChR2). However, some potential clinical applications of the optogenetic implant rely on other opsins, e.g. 470-490nm for anion-conducting channelrhodopsin GtACR [57], and 570-595nm for chloride ion-pumping rhodopsin halorhodopsin [58]. It is not that difficult to transfer the model from 470nm to other wavelength. Wavelength itself is a variable input parameter, so variations could be made by updating the scattering and absorption properties in the following optical and thermal analyses. As for the opto-neuro analyses, the 4-state model is common-used for the ChR2 family and is applicable for ion-channel rhodopsins by altering time constant and conductance. The introducing of different opsin types, e.g. halorhodopsin does bring the new photocycle and corresponding dynamics. However, the transition rate model is general so the photocycle dynamics in our opto-neuro analyses could be adjusted by replacing the ChR2 model with other opsin model, as far as the model has been developed. As the photocycle of halorhodopsin was reported recently [59], we would be glad to investigate its feasibility in developing optogenetic neural prosthetic system. 570-595nm yellow light is superior to the 470-490nm blue one, 1/1000 in the capability of tissue damage, and less scattering, and deeper penetrating depth

VI. CONCLUSION

In this paper, we proposed an optogenetic multiphysical fields coupling (OMFC) model for optogenetic implantable neuroprosthetic probes. The OMFC model summarised the reported modelling work for optogenetic neuroprosthetics. It was established by compositing three analyses for optical, thermal and optogenetic electrophysiological processes, based on the energy equivalence and exchange among different physical fields.

To validate the model, optogenetic implantable neuroprosthetic test probes based on miniature LEDs were developed. Then, optical, thermal measurement and neural photocurrent recording experiments were implemented on the test probes. By comparing the simulation and experiment results, we validated and calibrated the OMFC model so that we believe it would enable us to obtain the optical, thermal and electrophysiological responses for a given probe. As so, the model could be helpful as an early-stage design tool to reduce experiment iteration, even to achieve ‘‘one-time experimental validation’’ once updated and operated in the realistic environments for clinical applications. Owing to the complexities

of neural system, further experimental investigations could be taken to improve the modelling parameters further.

ACKNOWLEDGMENT

The authors declare that they have no other competing interests.

REFERENCES

[1] G. Nagel, T. Szellas, W. Huhn, S. Kateriya, N. Adeishvili, P. Berthold, D. Ollig, P. Hegemann, and E. Bamberg, "Channelrhodopsin-2, a directly light-gated cation-selective membrane channel," *Proc. Nat. Acad. Sci. USA*, vol. 100, no. 24, pp. 13940–13945, Nov. 2003.

[2] (2015). *RST-001 Phase I/II Trial for Advanced Retinitis Pigmentosa (Identifier: NCT02556736)*. [Online]. Available: http://ClinicalTrials.gov

[3] J.-A. Sahel, E. Boulanger-Scemama, C. Pagot, A. Arleo, F. Galluppi, J. N. Martel, S. D. Esposti, A. Delaux, J.-B. de Saint Aubert, C. de Montleau, E. Gutman, I. Audo, J. Duebel, S. Picaud, D. Dalkara, L. Blouin, M. Taiel, and B. Roska, "Partial recovery of visual function in a blind patient after optogenetic therapy," *Nature Med.*, vol. 27, no. 7, pp. 1223–1229, Jul. 2021.

[4] I. Reutsky-Gefen, L. Golan, N. Farah, A. Schejter, L. Tsur, I. Brosh, and S. Shoham, "Holographic optogenetic stimulation of patterned neuronal activity for vision restoration," *Nature Commun.*, vol. 4, no. 1, p. 1509, Feb. 2013.

[5] A. Soltan, J. M. Barrett, P. Maaskant, N. Armstrong, W. Al-Atabany, L. Chaudet, M. Neil, E. Sernagor, and P. Degenaar, "A head mounted device stimulator for optogenetic retinal prosthesis," *J. Neural Eng.*, vol. 15, no. 6, Dec. 2018, Art. no. 065002.

[6] Z. Zhang, L. E. Russell, A. M. Packer, O. M. Gauld, and M. Häusser, "Closed-loop all-optical interrogation of neural circuits in vivo," *Nature Methods*, vol. 15, no. 12, pp. 1037–1040, Dec. 2018.

[7] L. Grosenick, J. H. Marshel, and K. Deisseroth, "Closed-loop and activity-guided optogenetic control," *Neuron*, vol. 86, no. 1, pp. 106–139, Apr. 2015.

[8] P. Selvaraj, J. W. Sleigh, H. E. Kirsch, and A. J. Szeri, "Closed-loop feedback control and bifurcation analysis of epileptiform activity via optogenetic stimulation in a mathematical model of human cortex," *Phys. Rev. E, Stat. Phys. Plasmas Fluids Relat. Interdiscip. Top.*, vol. 93, no. 1, Jan. 2016, Art. no. 012416.

[9] E. Krook-Magnuson, C. Armstrong, M. Oijala, and I. Soltesz, "On-demand optogenetic control of spontaneous seizures in temporal lobe epilepsy," *Nature Commun.*, vol. 4, no. 1, p. 8, Jan. 2013.

[10] A. M. Aravanis, L.-P. Wang, F. Zhang, L. A. Meltzer, M. Z. Mogri, M. B. Schneider, and K. Deisseroth, "An optical neural interface: In vivo control of rodent motor cortex with integrated fiberoptic and optogenetic technology," *J. Neural Eng.*, vol. 4, no. 3, pp. S143–S156, Sep. 2007.

[11] H. Zhao, A. Soltan, P. Maaskant, N. Dong, X. Sun, and P. Degenaar, "A scalable optoelectronic neural probe architecture with self-diagnostic capability," *IEEE Trans. Circuits Syst. I, Reg. Papers*, vol. 65, no. 8, pp. 2431–2442, Aug. 2018.

[12] E. Segev, J. Reimer, L. C. Moreaux, T. M. Fowler, D. Chi, W. D. Sacher, M. Lo, K. Deisseroth, A. S. Tolias, A. Faraon, and M. L. Roukes, "Patterned photostimulation via visible-wavelength photonic probes for deep brain optogenetics," *Neurophotonics*, vol. 4, no. 1, p. 1, Dec. 2016.

[13] N. Dong, R. Berlinguer-Palmini, A. Soltan, N. Ponon, A. O'Neil, A. Travelyan, P. Maaskant, P. Degenaar, and X. Sun, "Opto-electro-thermal optimization of photonic probes for optogenetic neural stimulation," *J. Biophotonics*, vol. 11, no. 10, Mar. 2018, Art. no. e201700358.

[14] M. Azimipour, R. Baumgartner, Y. Liu, S. L. Jacques, K. Eliceiri, and R. Pashaie, "Extraction of optical properties and prediction of light distribution in rat brain tissue," *J. Biomed. Opt.*, vol. 19, no. 7, Jul. 2014, Art. no. 075001.

[15] M. Azimipour, F. Atry, and R. Pashaie, "Effect of blood vessels on light distribution in optogenetic stimulation of cortex," *Opt. Lett.*, vol. 40, no. 10, p. 2173, 2015.

[16] G. Yona, N. Meitav, I. Kahn, and S. Shoham, "Realistic numerical and analytical modeling of light scattering in brain tissue for optogenetic applications," *Eneuro*, vol. 3, no. 1, Jan. 2016., doi: 10.1523/ENEURO.0059-15.2015.

[17] N. McAlinden, D. Massoubre, E. Richardson, E. Gu, S. Sakata, M. D. Dawson, and K. Mathieson, "Thermal and optical characterization of micro-LED probes for in vivo optogenetic neural stimulation," *Opt. Lett.*, vol. 38, no. 6, pp. 992–994, 2013.

[18] J. M. Stujenske, T. Spellman, and J. A. Gordon, "Modeling the spatiotemporal dynamics of light and heat propagation for in vivo optogenetics," *Cell Rep.*, vol. 12, no. 3, pp. 525–534, Jul. 2015.

[19] A. Dubois, C.-C. Chiang, F. Smekens, S. Jan, V. Cuplov, S. Palfi, K.-S. Chuang, S. Senova, and F. Pain, "Optical and thermal simulations for the design of optodes for minimally invasive optogenetics stimulation or photomodulation of deep and large cortical areas in non-human primate brain," *J. Neural Eng.*, vol. 15, no. 6, Dec. 2018, Art. no. 065004.

[20] F. Dehkhoda, A. Soltan, N. Ponon, A. O'Neill, A. Jackson, and P. Degenaar, "A current-mode system to self-measure temperature on implantable optoelectronics," *Biomed. Eng. OnLine*, vol. 18, no. 1, p. 15, Dec. 2019.

[21] F. Dehkhoda, A. Soltan, N. Ponon, A. Jackson, A. O'Neill, and P. Degenaar, "Self-sensing of temperature rises on light emitting diode based optrodes," *J. Neural Eng.*, vol. 15, no. 2, Apr. 2018, Art. no. 026012.

[22] H. E. Kato, Y. S. Kim, J. M. Paggi, K. E. Evans, W. E. Allen, C. Richardson, K. Inoue, S. Ito, C. Ramakrishnan, L. E. Fenno, K. Yamashita, D. Hilger, S. Y. Lee, A. Berndt, K. Shen, H. Kandori, R. O. Dror, B. K. Kobilka, and K. Deisseroth, "Structural mechanisms of selectivity and gating in anion channelrhodopsins," *Nature*, vol. 561, no. 7723, pp. 349–354, Sep. 2018.

[23] K. Nikolic, N. Grossman, M. S. Grubb, J. Burrone, C. Toumazou, and P. Degenaar, "Photocycles of channelrhodopsin-2," *Photochem. Photobiol.*, vol. 85, no. 1, pp. 400–411, 2009.

[24] N. Grossman, K. Nikolic, C. Toumazou, and P. Degenaar, "Modeling study of the light stimulation of a neuron cell with channelrhodopsin-2 mutants," *IEEE Trans. Biomed. Eng.*, vol. 58, no. 6, pp. 1742–1751, Jun. 2011.

[25] N. Grossman, V. Simiaki, C. Martinet, C. Toumazou, S. R. Schultz, and K. Nikolic, "The spatial pattern of light determines the kinetics and modulates backpropagation of optogenetic action potentials," *J. Comput. Neurosci.*, vol. 34, no. 3, pp. 477–488, Jun. 2013.

[26] Z. Shen, H. Zhang, Z. Cao, L. Yan, Y. Zhao, L. Du, and Z. Deng, "Transition dynamics and optogenetic controls of generalized periodic epileptiform discharges," *Neural Netw.*, vol. 149, pp. 1–17, May 2022.

[27] L. Zhang, Z. Ma, Y. Yu, B. Li, S. Wu, Y. Liu, and G. Baier, "Examining the low-voltage fast seizure-onset and its response to optogenetic stimulation in a biophysical network model of the hippocampus," *Cognit. Neurodyn.*, vol. 18, no. 1, pp. 265–282, Feb.10, 2023.

[28] H. M. Peixoto, R. M. S. Cruz, T. C. Moulin, and R. N. Leão, "Modeling the effect of temperature on membrane response of light stimulation in optogenetically-targeted neurons," *Frontiers Comput. Neurosci.*, vol. 14, p. 5, Feb. 2020, doi: 10.3389/fncom.2020.00005.

[29] J. Luo, D. Firflionis, M. Turnbull, W. Xu, D. Walsh, E. Escobedo-Cousin, A. Soltan, R. Ramezani, Y. Liu, R. Bailey, A. O'Neill, A. S. Idil, N. Donaldson, T. Constandinou, A. Jackson, and P. Degenaar, "The neural engine: A reprogrammable low power platform for closed-loop optogenetics," *IEEE Trans. Biomed. Eng.*, vol. 67, no. 11, pp. 3004–3015, Nov. 2020.

[30] B. Zaaimi et al., "Closed-loop optogenetic control of the dynamics of neural activity in non-human primates," *Nature Biomed. Eng.*, vol. 7, no. 4, pp. 559–575, Oct. 2022.

[31] N. Dong, W. Jiang, and X. Sun, "Variable spatial pattern probe based on offset launch of multimode waveguide for optogenetics," *Opt. Exp.*, vol. 24, no. 10, p. 10921, May 2016.

[32] Y. Son, H. J. Lee, J. Kim, H. Shin, N. Choi, C. J. Lee, E.-S. Yoon, E. Yoon, K. D. Wise, T. G. Kim, and I.-J. Cho, "In vivo optical modulation of neural signals using monolithically integrated two-dimensional neural probe arrays," *Sci. Rep.*, vol. 5, no. 1, p. 11, Oct. 2015.

[33] A. K. Dunn, "Optical properties of neural tissue," in *Optical Imaging of Neocortical Dynamics*, vol. 3, 1st ed., F. H. B. Weber, Ed., Totowa, NJ, USA: Humana Press, 2014, pp. 31–55.

[34] F. Bevilacqua, D. Piguet, P. Marquet, J. D. Gross, B. J. Tromberg, and C. Depeursinge, "In vivo local determination of tissue optical properties: Applications to human brain," *Appl. Opt.*, vol. 38, no. 22, p. 4939, Aug. 1999.

[35] S. L. Jacques, "Optical properties of biological tissues: A review," *Phys. Med. Biol.*, vol. 58, no. 11, pp. R37–R61, Jun. 2013.

[36] P. Hegemann and A. Möglich, "Channelrhodopsin engineering and exploration of new optogenetic tools," *Nature Methods*, vol. 8, no. 1, pp. 39–42, Jan. 2011.

[37] O. P. Ernst, D. T. Lodowski, M. Elstner, P. Hegemann, L. S. Brown, and H. Kandori, "Microbial and animal rhodopsins: Structures, functions, and molecular mechanisms," *Chem. Rev.*, vol. 114, no. 1, pp. 126–163, Jan. 2014.

[38] R. R. Birge and T. M. Cooper, "Energy storage in the primary step of the photocycle of bacteriorhodopsin," *Biophys. J.*, vol. 42, no. 1, pp. 61–69, Apr. 1983.

[39] S. Kleinlogel, K. Feldbauer, R. E. Dempski, H. Fotis, P. G. Wood, C. Bamann, and E. Bamberg, "Ultra light-sensitive and fast neuronal activation with the Ca^{2+}-permeable channelrhodopsin CatCh," *Nature Neurosci.*, vol. 14, no. 4, pp. 513–518, Apr. 2011.

[40] J. Luo, K. Nikolic, B. D. Evans, N. Dong, X. Sun, P. Andras, A. Yakovlev, and P. Degenaar, "Optogenetics in silicon: A neural processor for predicting optically active neural networks," *IEEE Trans. Biomed. Circuits Syst.*, vol. 11, no. 1, pp. 15–27, Feb. 2017.

[41] J. Kuhne, J. Vierock, S. A. Tennigkeit, M.-A. Dreier, J. Wietek, D. Petersen, K. Gavriljuk, S. F. El-Mashtoly, P. Hegemann, and K. Gerwert, "Unifying photocycle model for light adaptation and temporal evolution of cation conductance in channelrhodopsin-2," *Proc. Nat. Acad. Sci. USA*, vol. 116, no. 19, pp. 9380–9389, May 2019.

[42] K. Koamoto, *Fundamentals of Optical Waveguides*. Burlington, MA, USA: Acacdemic, 2006.

[43] M. Born and E. Wolf, *Principle of Optics: Electromagnetic Theory of Propagation, Interference and Diffraction of Light*, 7th ed., Cambridge, U.K.: Cambridge Univ. Press, 1999.

[44] C. F. Bohren and D. R. Huffman, *Absorption and Scattering of Light by Small Particles*, 1st ed., Weinheim, Germany: Wiley, 1998, p. 544.

[45] A. Bhandari, B. Hamre, Ø. Frette, K. Stamnes, and J. J. Stamnes, "Modeling optical properties of human skin using mie theory for particles with different size distributions and refractive indices," *Opt. Exp.*, vol. 19, no. 15, p. 14549, 2011.

[46] C. Zhu and Q. Liu, "Review of Monte Carlo modeling of light transport in tissues," *J. Biomed. Opt.*, vol. 18, no. 5, May 2013, Art. no. 050902.

[47] J. Werner and M. Buse, "Temperature profiles with respect to inhomogeneity and geometry of the human body," *J. Appl. Physiol.*, vol. 65, no. 3, pp. 1110–1118, Sep. 1988.

[48] H. H. Pennes, "Analysis of tissue and arterial blood temperatures in the resting human forearm," *J. Appl. Physiol.*, vol. 85, no. 1, pp. 5–34, Jul. 1998.

[49] Y. A. Cengel and Y. Cengel, *Heat, Heat Transfer, A Practical Approach With Solutions Manual*. New York, NY, USA: McGraw-Hill, 2003.

[50] S. F. Owen, M. H. Liu, and A. C. Kreitzer, "Thermal constraints on in vivo optogenetic manipulations," *Nature Neurosci.*, vol. 22, no. 7, pp. 1061–1065, Jul. 2019.

[51] K. Ait Ouares, C. Beurrier, M. Canepari, G. Laverne, and N. Kuczewski, "Opto nongenetics inhibition of neuronal firing," *Eur. J. Neurosci.*, vol. 49, no. 1, pp. 6–26, Jan. 2019.

[52] P. J. Stiles and C. G. Gray, "Improved Hodgkin–Huxley type model for neural action potentials," *Eur. Biophys. J.*, vol. 50, no. 6, pp. 819–828, Sep. 2021.

[53] Y. Wu, Q. Ding, T. Li, D. Yu, and Y. Jia, "Effect of temperature on synchronization of scale-free neuronal network," *Nonlinear Dyn.*, vol. 111, no. 3, pp. 2693–2710, Feb. 2023.

[54] *Implants for Surgery—Active Implantable Medical Devices—Part 1: General Requirements for Safety, Marking and for Information to be Provided by the Manufacturer*, Int. Org. Standardization, Geneva, Switzerland, 2014.

[55] S. I. Al-Juboori, A. Dondzillo, E. A. Stubblefield, G. Felsen, T. C. Lei, and A. Klug, "Light scattering properties vary across different regions of the adult mouse brain," *PLoS ONE*, vol. 8, no. 7, Jul. 2013, Art. no. e67626.

[56] N. A. Steinmetz et al., "Neuropixels 2.0: A sminiaturised high-density probe for stable, long-term brain recordings," *Science*, vol. 372, no. 6539, Apr. 2021, Art. no. eabf4588.

[57] M. Mahn, L. Gibor, P. Patil, K. Cohen-Kashi Malina, S. Oring, Y. Printz, R. Levy, I. Lampl, and O. Yizhar, "High-efficiency optogenetic silencing with soma-targeted anion-conducting channelrhodopsins," *Nature Commun.*, vol. 9, no. 1, p. 4125, Oct. 2018.

[58] R. C. Wykes, D. M. Kullmann, I. Pavlov, and V. Magloire, "Optogenetic approaches to treat epilepsy," *J. Neurosci. Methods*, vol. 260, pp. 215–220, Feb.15, 2016.

[59] H. Feroz, B. Ferlez, C. Lefoulon, T. Ren, C. S. Baker, J. P. Gajewski, D. J. Lugar, S. B. Gaudana, P. J. Butler, J. Hühn, M. Lamping, W. J. Parak, J. M. Hibberd, C. A. Kerfeld, N. Smirnoff, M. R. Blatt, J. H. Golbeck, and M. Kumar, "Light-driven chloride transport kinetics of halorhodopsin," *Biophys. J.*, vol. 115, no. 2, pp. 353–360, Jul. 2018.

NA DONG received the B.S. and Ph.D. degrees in electronics engineering from Southeast University, Nanjing, China, in 2011 and 2018, respectively.

He has been an Assistant Research Professor with the College of Electronics Science and Engineering, Southeast University, since 2019. His research interests include biomedical optics and multi-physical biophysical modeling of device-tissue interface for neuroprosthesis.

EMILY JOHNSON received the B.Sc. degree (Hons.) in neuroscience and the Ph.D. degree from the University of Leeds, with a focus on the role of T-type Ca^{2+} channels in proliferative cardiovascular disease. Then she spent five years as a Postdoctoral Research Fellow, utilizing her expertise with patch-clamp electrophysiology, optogenetics, and 2-photon Ca^{2+} imaging, to address novel Neuroscience research questions. She is a natural problem solver and a collaborative Researcher and she has a tenacious attitude useful for acquiring high-quality and reproducible data. She is currently a member of the Ion Channel Laboratory, ApconiX.

ROLANDO BERLINGUER-PALMINI received the degree in biological sciences mastered in molecular biology and the Ph.D. degree in physiological and nutritional sciences from the University of Florence, Italy, in 1998 and 2004, respectively. In 2008, he moved to London as a Research Associate on the OptoNeuro Project, first at Imperial College, and then at Newcastle University. He is currently the Experimental Scientific Officer of the Bio-Imaging Unit, Newcastle University, U.K. His major specialty is super-resolution microscopy for bio-imaging and advanced image analyses methods and workflows.

HONGZE ZHONG received the M.Sc. degree from Newcastle University, U.K., in 2019, where he is currently pursuing the Ph.D. degree, under the supervision of Dr. Patrick Degenaar, with a focus on biophysical modeling. He is a Medical Physicist in China.

FAHIMEH DEHKHODA received the M.Sc. and Ph.D. degrees in electrical engineering from the University of Tabriz, Tabriz, Iran, in 2004 and 2012, respectively. She was a Visiting Researcher with the Centre of Biomedical Engineering, The University of Adelaide, Adelaide, SA, Australia, from 2010 to 2011, involved in multichannel receiver for micro-MRI. She joined CANDO Project, in 2014, to work on implantable electronics with the School of Engineering, Newcastle University, Newcastle upon Tyne, U.K. She is currently a Research Associate with the School of Engineering, The University of Edinburgh, Edinburgh, U.K., involved in CMOS design for SPAD sensors in QuantIC Project. Her research interests include biomedical implantable CMOS and sensor interface, CMOS-based spectroscopy, and SPAD imaging systems.

AHMED SOLTAN received the B.Sc. and M.Sc. degrees and the Ph.D. degree in electronics and communication from Cairo University, Cairo, Egypt, in 2004, 2008, and 2014, respectively. He was involved in circuit and system design and modeling in the fractional order domain during the Ph.D. research. He was a Research Associate and an EDA/CAD Specialist with the School of Engineering, Newcastle University, U.K. He was a Teacher Assistant with the Faculty of Engineering, Fayoum University, Faiyum, Egypt, for nine years, and a Research and Development Firmware Engineer for eight years. He was the Research and Development Manager of an LED company in Qatar, for one year and a half. He is currently an Associate Professor with Nile University, Egypt. His research interests include the thermal impact of the implantable devices on human tissues, embedded system design for lab-on-chip systems, and the investigation of fractional circuits and systems, specifically in fractional order analog filters for signal processing and fractional order modeling for biomedical applications. Aiming at establishing a new healthcare monitoring system and diagnosis on the fly by the development of autonomous devices, his current research interests include smart energy harvesting systems and power management for biomedical implantable devices and lab-on-chip systems.

KONSTANTIN NIKOLIC (Member, IEEE) received the degree and master's degree in applied physics from the University of Belgrade, Serbia, and the Ph.D. degree in physics from Imperial College London, London, U.K. He has been a Professor of computer science: AI, machine learning, and data science with the School of Computing and Engineering, University of West London, since February 2020. He is currently a Visiting Professor with the Department of Electrical and Electronic Engineering, Imperial College London. Previously, he was a Research Fellow, then a Senior Research Fellow and the Principal Investigator of the Institute of Biomedical Engineering and the Department of Electrical and Electronic Engineering, Imperial College London, from June 2006 to February 2020. Before that, he was a Senior Research Associate with UCL, and an Assistant Professor and then an Associate Professor with the Faculty of Electrical Engineering, University of Belgrade. He leads NeuroAI Group, which develops methods and computational tools for understanding, modeling, and simulating various biological and physiological processes, and their applications in AI/ML, bio-inspired electronic systems, and diagnostics. He is a member of the IEEE CAS Technical Committee and the Royal Society Neural Interfaces Steering Group. He is an Associate Editor of *Frontiers in Neuroscience* and *Frontiers in Neuromorphic Engineering* and previously IEEE TRANSACTIONS ON BIOMEDICAL CIRCUITS AND SYSTEMS.

NIR GROSSMAN received the B.Sc. degree in physics from Israel Institute of Technology (Technion), the M.Sc. degree in electromagnetic engineering from the Technical University of Hamburg-Harburg (TUHH), Germany, and the Ph.D. degree in neuroscience from Imperial College London. He joined the Christofer Toumazou's Laboratory, Institute of Biomedical Engineering, Imperial College London. He joined Ed Boyden's Laboratory, MIT's Media Laboratory, the McGovern Institute for Brain Research, and the Alvaro Pascual-Leone's Laboratory, Harvard's Berenson-Allen Center for Noninvasive Brain Stimulation. He then returned to Imperial College London and joined the Centre for Bio-Inspired Technology, Department of Electrical and Electronic Engineering, before joining the Faculty of Medicine. He develops neuromodulatory interventions for brain disorders by pioneering new tools and principles to impact the disease pathology via direct modulation of the underlying aberrant neural activity. His research drives innovation through rigorous scientific exploration of common biophysical principles and rules underpinning the neural processing of electromagnetic stimulation, using natural bridges between advanced computational neuroscience and cutting-edge experiments, ranging from a single neuron cell to human behavior. Following the Ph.D. degree, he was awarded the BBSRC (Biotechnology and Biological Sciences Research Council) Enterprise Fellowship. After the completion of the BBSRC Fellowship, he was awarded the Wellcome Trust MIT Fellowship.

JOHANNES GAUSDEN received the Ph.D. degree from Newcastle University, in 2020. He is currently a Research Associate of bioelectronics with the School of Engineering, Newcastle University. He specializes in the development of microfabricated medical probes. In particular, he was involved in the CANDO Project, where he helped to develop a 3 dimensional photonic probe for optical neural stimulation. More recently, he has been working on flexible electrical probes for peripheral muscle stimulation.

RICHARD BAILEY received the Ph.D. degree. He is currently a Research Associate with the School of Engineering, Newcastle University. His research interests include microfabrication; surface analysis; microscopy; cell structure, growth, and division; cell mechanics and physical properties; microbiology; and materials science.

ANTHONY O'NEILL (Senior Member, IEEE) joined Newcastle University, in 1986, where he has been a Siemens Professor of microelectronics, since 1996, and previously with Plessey Research (Caswell) Ltd. In 1994, he was a Visiting Scientist with MIT, Cambridge, MA, USA. In 2002, he became a Royal Society Industry Fellow with Atmel, U.K. He was a Visiting Professor with EPFL, Lausanne, Switzerland, in 2009, and Monash University, Melbourne, Australia, in 2017. His research interests include device fabrication in cleanrooms, specialist electrical and material characterization, computer simulation (e.g. TCAD), and electronic systems. His memberships include a Chartered Engineer, and a fellow of IET.

ANDREW JACKSON received the Ph.D. degree in neuroscience from University College London. Then he pursued post-doctoral research with the University of Washington, USA. He is currently a Professor of neural interfaces with Newcastle University. He is also a Senior Research Fellow with the Wellcome Trust and a member with INSPIRE's NSC Andrew Trevelyan. He is a Professor of network neuroscience with Newcastle University. His research interests include movement neuroscience, epilepsy, sleep, neurotechnology, neural prosthetics, brain–machine interfaces, and how the brain regulates its activity levels, specifically, he has focused upon the neocortex and hippocampus, which are the parts of the brain concerned with higher cognitive function. These are also the parts of the brain that are susceptible to epileptic activity and a major part of his research involves trying to understand how and why epileptic seizures occur. He is a Clinically Trained Researcher and worked briefly as a Junior Neurologist and a Neurosurgeon, although he no longer practices clinical medicine, choosing instead to do full-time neuroscientific research. He is a Current Member of the Scientific Advisory Committee for Epilepsy Research, U.K. He has held personal fellowships for his epilepsy work on both sides of the Atlantic and was awarded the Schaefer Scholarship at Columbia University in 2016.

PATRICK DEGENAAR (Senior Member, IEEE) received the bachelor's degree (Hons.) in applied physics and the M.Res. degree in surface science from Liverpool University, Liverpool, U.K., in 1996 and 1997, respectively, and the Ph.D. degree in bioimaging from Japan Advanced Institute of Science and Technology, Ishikawa, Japan, in 2001. The Post-Ph.D. degree, he initially worked in the software industry, then joined Imperial College, London as a Postdoctoral Researcher. In 2005, he received the RCUK Fellowship and a Lectureship. He advanced to a Senior Lectureship before joining Newcastle University, in 2010, where he became a Full Professor of neuroprosthetics, in 2019. His research interests include the crossover between neuroscience optoelectronics and device engineering. He has a specific interest in developing optogenetic forms of visual prosthetics for the limited vision. His memberships include IEEE, IOP, ARVO, SPIE, and BioCAS.

XIAOHAN SUN was a Visiting Professor with the Research Laboratory of Electronics, Massachusetts Institute of Technology, Cambridge, MA, USA, from 2002 to 2004. She is currently a Professor with the Department of Electronics Engineering and the Director of the National Research Center for Optical Sensing/Communications Integrated Networking, Southeast University, Nanjing, China. Her research interests include photonic/electronic hybrid integrated chips and devices, optical sensing, and next-generation optical networks.